Accretion disc boundary layers around pre-main sequence stars

Patrick Godon
NASA/Jet Propulsion *[laboratory, 4800 Oak Grove Dr., MS 2.?8-332, Pasadena, CA 91109*

ABSTRACT

One-dimensional time dependent calculations of geometrically thin accretion discs boundary layers in pre-main sequence stars arc carried out for mass accretion rates in the range $\dot{M} = 5 \times 10^{-7}$ - $10^{-4} M_\odot/y$, $\alpha = 0.005$- 0.3 and different inner boundary conditions on the temperature. Two kinds of solutions arc obtained: solutions with a distinct thermal boundary layer component and solution without thermal boundary layer. For $\dot{M}$ up to $\approx 10^{-5} M_\odot/y$, and for $\alpha > \alpha_{critic} \approx 0.04$, solutions with a thermal BL arc obtained. For M $\approx 10^{-4} M_\odot/y$ *or* for $\alpha < \alpha_{critic}$, solutions without a thermal BL arc obtained. The inner boundary condition $F_r = \sigma T_{eff}^4$ leads to hotter solutions and higher threshold values α_{critic}, while the non-flux boundary condition $dT/dr = 0$ leads to cooler solutions. For very low mass accretion rate ($\dot{M} \approx 5 \times 10^{-7} M_\odot/y$), the temperature in the disc drops below 10^4K and the ionization front is adjacent to the outer edge of the hot thermal boundary layer. In the vicinity of the ionization front, the medium becomes slightly optically thin.

Key words: accretion, accretion discs - methods: numerical

1 INTRODUCTION

It is now commonly believed that TTauri systems are stars in early stage of evolution: pre-main sequence stars accreting matter from a disc, remanent of a protostellar cloud. Circumstellar gas around TTauri stars has indeed been detected in the radio frequencies (Sargent and Beckwith, 1991) and in several cases, the velocity field of the circumstellar gas appears to be consistent with that of a Keplerian disc (Koerner, Sargent and Beckwith 1993, Koerner and Sargent. 1995). TTauri stars spectra, furthermore, display strong ultraviolet and infrared excesses when compared to main sequence stars of similar spectral type. In order to reproduce the observed spectral shapes and continuum of TTauri stars, accretion discs with Boundary Layers (BL) have been invoked with mass accretion rates in the range $\dot{M} \approx 1\ 0^{-9} M_\odot/y$ up to $5 \times 10^{-7} M_\odot/y$ (Bertout, Basri and Bouvier 1988, Hartigan et al. 1989, Basri and Bertout 1989, Hartigan et al. 1991, Bouvier and Bertout 1992, Bertout et al. 1993). These models take into account the luminosity of the star, the BL and disc (including absorbed stellar flux). They all suggest BL temperatures $7000K < T_{BL} < 11000K$ and $\dot{M} \approx 10^{-7}\ MO/y$. It seems that in this regime of M, the BL becomes optically thin (Basri and Bertout 1989, Hartigan et al. 1989). Obviously, accretion discs BLs modeling is strongly needed in order to model the spectra of TTauri stars. First results of steady state calculations of BL models (Popham et at. 1993, Lioure and Le Contel 1994 and Regev and Bertout 1995) arc in agreement with the observations. The results show a strong dependence on physical assumptions such as the inner boundary conditions on the temperature, the value of the viscosity parameter α and even the method of solution (Regev and Bertout 1995). Furthermore, a major subject of concern in modeling is the opacity law, which treatment has been neglected in the low temperature r egime (Popham et al. 1993, Lioure and Le Contel 1994), therefore, making these models inadequate to reproduce the effects of the opacity "gap" on the cool solutions, characteristic of the low mass accretion rate models.

Modeling of accretion discs BLs in pre-main sequence stars is also important to understand the FU Orionis objects. These systems ar e believed to be TTauri stars which undergo outburst and i, icr-case their mass accretion rate by several orders of magnitude, from $\dot{M} \approx 10^{-7} M_\odot/y$ up to M $\approx 10^{-4} M_\odot/y$ (Lin and Papaloizou 1985). Treatments of Fu Orionis do not include BL regions, but instead it is assumed that the disc extends up to the stellar surface (Kenyon, Hartmann and Hewett 1988). Stability analysis (Clarke, Lin and Paploizou 1989, Clarke, Lin and Pringle 1990) have shown that the pert urbation of a low mass accretion rate disc around a TTauri star can produce FU Orionis behaviour, by triggering the thermal ionization instability when the disc mid-plane is partially ionized at some intermediate radius (Lin and Pa-

paloizou 1985). These systems have an ionization front which separates hot (ionized) phase from cool (neutral) one. Obviously, the opacity decreases by several orders of magnitude ("gap") as one moves from the hot region ($T > 10^4 K$) to the cooler one ($T < 10^4$ K). Time dependent models (Bells, Lin and Ruden 1991, Bell and Lin 1994 and Bell et al. 1995) have been invoked to reproduce the rising and falling luminosity curves of FU Orionis during outburst. These models assume a Keplerian disc, without BL, with mass accretion rate $\dot{M} = (1 - 10) \times 10^{-6} M_\odot/y$ and $\alpha = 10^{-3}$, 10^{-4}, in order to fit the observed time dependent light curves of FU Orionis outburst .

It is the purpose of this paper to provide more details on the inner part of the disc in pre-main sequence stars. The BL is important not only because up to half the accretion energy can be released there, but mainly because the standard disc model is not appropriate when $\Omega \neq \Omega_K, F_r \neq 0$, $\nu_{BL} << \nu_{disc}$ and $\Sigma_{BL} << \Sigma_{disc}$. This is especially true when $\dot{M}$ is large and α is small (like in FU Orionis, Bell et al. 1995). In this case the non-Keplerian inner part of the disc extends outward up to several stellar radii (Popham et al. 1993 and the results presented here). In the present work, time dependent numerical calculations of one-dimensional accretion disc BL around pre-main sequence stars are carried out. The method is based on a Chebyshev spectral method used previously to model accretion BL around white dwarf in Cataclysmic Variable systems (Go don 1995a, and Godon, Regev and Shaviv 1995), and it has been implemented to treat discs around pm-main sequence stars. The opacity law has been given a full treatment, in order to reproduce the effects of the opacity gap on the solutions: the formation of an outer cool and neutral region.

The equations and the physical assumptions of the modeling are presented in section 2. The numerical method used to solve the equations is described in section 3. The results of the numerical calculations appears in the 4th section and are discussed in the 5th section.

2 EQUATIONS AND ASSUMPTIONS

2.1 Equations

The full Navier-Stokes equations are solved including the gravity of the star, viscosity and radiative transfer treated in the diffusion approximation. In the high temperature regime, the effect of radiation pressure is included in the Equation of State; while in the low temperature regime Saha's equation is used to write the equation of a partially ionized Hydrogen gas. The treatment is one dimensional and the equations are written in cylindrical coordinates (r, z, ϕ). Axi-symmetry is assumed around the z- axis ($\frac{\partial}{\partial \phi} = 0$). The disc and the BL are assumed to be in hydrostatic equilibrium and geometrically thin in the vertical direction. Following the usual procedure, the equations are solved for the z-integrated variables. The exact form of the equations and the physical assumptions can be found in Godon et al. (1995). The equations for the integrated quantities have the following form:

the conservation of maw

$$\frac{\partial \Sigma}{\partial t} = -\frac{1}{r}\frac{\partial}{\partial r}(r\Sigma v_r), \tag{1}$$

the conservation of radial momentum

$$\frac{\partial}{\partial t}(v_r\Sigma) = -\frac{1}{r}\frac{\partial}{\partial r}[r v_r(v_r\Sigma)] + r\Sigma\Omega^2 - \Sigma\frac{GM}{r^2} - \frac{\partial P}{\partial r} + F_\nu, \tag{2}$$

the conservation of angular momentum

$$\frac{\partial}{\partial t}(\Sigma r^2\Omega) = -\frac{1}{r}\frac{\partial}{\partial r}(r\Sigma r^2\Omega v_r) + \frac{1}{r}\frac{\partial}{\partial r}(r^3\nu\Sigma\frac{\partial\Omega}{\partial r}), \tag{3}$$

and the conservation of energy

$$\Sigma T\frac{\partial S}{\partial t} = -\Sigma T v_r\frac{\partial S}{\partial r} + \nu\Sigma(r\frac{\partial\Omega}{\partial r})^2 - \frac{4acT^4}{3\kappa\Sigma} + \frac{16ac}{3r}\frac{\partial}{\partial r}\left[\frac{rH^2T^3}{\kappa\Sigma}\frac{\partial T}{\partial r}\right] \tag{4}$$

where $\Sigma = \int_{-H(r)}^{+H(r)} \rho dz$, v_r is the radial velocity, Ω is the angular velocity, G is the gravity constant, M is the mass of the star, S is the entropy, a is the Stephan-Boltzmann constant, c is the speed of light, T is the mid-plane temperature, H is the half thickness of the disc and κ is the opacity law. An average value of the central density ρ_c is defined through the relation $\Sigma = 2H(r)\rho_c$. The pressure includes the gas and the radiation:

$$P = \frac{\Sigma\mathcal{R}T}{\mu} + \frac{1}{3}2Ha T^4.$$

The radial viscous force F_ν is:

$$F_\nu = \frac{\partial}{\partial r}\left[\frac{4\nu_r\Sigma}{3r}\frac{\partial(rv_r)}{\partial r}\right] - 2\frac{v_r}{r}\frac{\partial(\nu_r\Sigma)}{\partial r},$$

where ν is the coefficient of the shear viscosity, ν_r is the coefficient of the viscosity in the equation of radial momentum, $\mathcal{R}$ is the gas constant and μ is the mean molecular weight.

2.2 Boundary conditions

The inner boundary of the computational domain is the rotating stellar surface (r =. R.) through which matter flows into the star at a constant rate ($\dot{\mathcal{M}}$). In the present work two different inner boundary conditions on the temperature are considered: first an effective photospheric temperature is assumed for the star $T_* = 5 \times 10^9 K$ and then the temperature gradient is chosen such that $F_r = \sigma T_*^4$; in the second case a non flux boundary condition $dT/dr = 0$ is imposed on the inner boundary. The outer boundary of the computational domain (located at r = 2R.) is the inner edge of the disc and rotates with the Keplerian velocity. The gas enters this boundary at the same rate as it leaves through the inner boundary ($\dot{\mathcal{M}}$).

2.3 Initial conditions

Since the equations are time dependent, initial conditions have to be specified. The initial conditions are the superposition of an isothermal atmosphere and an inflowing disc of matter. The initial pressure is given through the equation of state. The initial radial momentum is obtained through the relation $\dot{M} = const.$ in some cases the steady state solutions obtained are used as initial conditions for other models.

2.4 Viscosity proscription

An α prescription is used for the viscosity (Shakura & Sunyaev, 1973) similar to the one originally used by Papaloizou & Stanley (1986), but with different approximations:

$$\nu = \alpha c_s \bar{H}, \tag{5}$$

where $c_s^2 = \Gamma_1 P/\rho$ is the sound speed, $\bar{H} = (H^{-2} + H_r^{-2})^{-1/2}$ and H_r is the pressure scale height in the radial direction $H_r = P(\partial P/\partial r)^{-1}$. For high radial infall velocities, the scale height $\bar{H}$ can be written:

$$\bar{H} = \frac{H}{\left[1 + \frac{r^2}{H^2}\left(\frac{1 - \frac{\Omega^2}{\Omega_K^2} - \frac{v_r^2}{r^2\Omega_K^2}}{1 - v_r^2/c_s^2}\right)^2\right]^{1/2}}. \tag{6}$$

This prescription leads to a viscosity which drops by ≈ 2 orders of magnitude in the region close to the stellar surface where the pressure gradient is high and the radial scale height is smaller than the vertical one.

To check the effect of the viscosity on the solution, a different α viscosity prescription, developed for non-Keplerian discs (Godon 1995b), is introduced in the calculations:

$$\nu = \alpha c_s H \mathcal{M}_t^2 \frac{\left|\frac{d\Omega_K}{dr}\right|}{\left|\frac{d\Omega}{dr}\right|}, \tag{7}$$

which can be written

$$\nu = \frac{\alpha v_t^2}{r\left|\frac{d\Omega}{dr}\right|}, \tag{8}$$

where $v_t = \mathcal{M}_t c_s$ is the turbulent velocity. Models with large values of α develop high radial velocities. For these particular cases the viscosity is modified using a coefficient developed from a causality formalism (Popham and Narayan 1992):

$$\nu \rightarrow \nu\left(1 - \frac{v_r^2}{\beta^2 c_s^2}\right)^2, \tag{9}$$

where $\beta = 1$ when $\mathcal{M}_t < 1$ and $\beta = \mathcal{M}_t$ otherwise. However, in the present calculations $\mathcal{M}_t = 1$ is assumed.

2.5 The opacity law

The opacity is an important factor in the modeling of accretion discs around young stellar objects (YSO). The abrupt jump in the opacity (which occurs around $T \approx 10^4$) can change drastically the nature of disc and gives rise to thermal instability responsible for the outbursts seen in FU Orionis stars. In these systems the "jump" appears in the ionization front located at several stellar radii (Bell et al. 1995). in cooler discs (with smaller mass accretion rates), one expects the ionization front to be located at smaller radii, not very far from the stellar surface and the hotter BL. It is, therefore, primordial to include the exact opacity law in models of accretion disc BL around YSOS and especially around the "cooler" T Tauri stars. In previous works (steady-state calculations of Popham et al. 1993 and Lioure and Le Contel 1994) the opacity gap is not included in the opacity law.

In this work an analytical form of the opacity is used, first developed by Lin and Papaloizou (1985), and then implemented by Bell and Lin (1994) in the range $T < 3000$K. The opacity (frequency averaged) is written

$$\kappa = \kappa_i \rho^{a_i} T^{b_i}, \tag{10}$$

where $i = 1, ..8$ accounts for eight different regimes of temperatures and densities (see Bell and Lin 1994 for more details). in figure 1 the opacity is drawn as a function of the temperature for different densities. The opacity "gap" occurs around $T = 10^4 K$ for practically all densities.

2.6 Optically thin case.

In those same models which required a precise description of the opacity gap, optically thin regions develops (see Results). Therefore, in these cases an adequate treatment of the radiation flux in the limit of optically thin medium is applied: a prescription similar to the one used in Popham et al, (1993), based on the analytical model of Hubeny (1990) a generalization of the Gray temperature distribution for stellar atmosphere applied to thin discs, under the assumption of Local Thermodynamic Equilibrium).

3 THE NUMERICAL METHOD

The spatial dependence of the equations is treated with a Chebyshev Spectral method, while a Crank-Nicholson and a second order Runge Kutta method are used for the time dependence of the equations. The numerical method has been widely described in Godon et al. (1995) and Godon (1995a).

3.1 The Spectral Methods

Details on the spectral methods can be found in Canuto et al. (1988), Gottlieb and Orszag (1977) and Voigt et al. (1984). Spectral methods are based on expanding the solution $u(x)$ (of eqs.1-4) in terms of a series of functions $\psi_n(x)$ (a complete set of orthogonal functions in a space S):

$$u_N(x) = \sum_{n=0}^{N} a_n \psi_n(x),$$

One replaces $u(x_j)$ by $u_N(x_j)$ in the solution of the initial problem (eqs. 1-4)

$$\frac{\partial u(x,t)}{\partial t} = L[u(x,t)] + f(x,t), \tag{11}$$

and defines the residue of the approximation u_N by :

$$R_N = \left\{\frac{\partial u_N}{\partial t} - L[u_N]\right\} - \left\{\frac{\partial u}{\partial t} - L[u]\right\}, \tag{12}$$

or

$$R_N = \frac{\partial u_N}{\partial t} - L[u_N] - f \tag{13}$$

This residue vanishes if u_N is the exact solution. One then minimizes R_N by projecting it on the basis $\psi_n(x)$ (n=0,1,.. N) (in a subspace S_N of S) and then by demanding that this projection vanishes,

$$P_N R_N = 0. \tag{14}$$

The projection operator, P_N, determines the spectra] method used and the approxi mation space, S_N, is determined by choice of the expansion polynomials.

3.2 The Chebyshev Pseudospectral method

The Chebyshev expansion is appropriate for nonperiodic boundary conditions and the repartition of the grid points is higher at the boundaries. The Chebyshev polynomials arc defined as

$$T_n(x) = cos[n\, arccos(x)], \qquad (15)$$

In this work the Chebyshev Pseudospectral method is used to evaluate the spatial derivatives of any function u. One expands u

$$u_N = \sum_{n=0}^{N} a_n T_n(x),$$

while a_n is given try

$$a_n = \frac{2}{N}\frac{1}{\bar{c}_n}\sum_{j=0}^{N}\frac{u_j}{\bar{c}_j}cos(\frac{\pi jn}{N}),$$

where $x_j = cos(\pi j/N), u_j = u(x_j)$ and $\bar{c}_0 = \bar{c}_N = 2$, $\bar{c}_j = 1$ for $0 < j$ </v.
Onc then differentiates the expression for UN

$$\frac{du_N}{dx} = \sum_{n=0}^{N} a_n T_n'(x),$$

and rewrite

$$\frac{du_N}{dx} = \sum_{n=0}^{N-1} a_n^{(1)} T_n(x).$$

The recurrent relations between $T_n'(x)$ and $T_n(x)$ leads to the following:

$$a_n^{(1)} = \frac{2}{c_n}\sum_{p=n+1,2}^{N-1} \cdot \cdot , \qquad n = 0, 1, .. N.$$

where $c_0 = 2$, c_j . 1 for O < j < N and p=n+1 ,2 means p=n+ 1 by 2.

4 RESULTS

In all numerical models presented here the accreting star has a radius $R_* = 4.3\, R_\odot$, mass $M = 1$ x MO and $\Omega_* = 0.1 \times \Omega_K(R_*)$. The parameters which arc changed from model to model arc the α viscosity parameter, the flux condition at the inner boundary and the mass accretion rate $\dot{M}$. All the models are listed in Table 1. In the first column the models arc denoted by 1,2,.. and J 1. In column *2* the value of the α viscosity parameter is given. The maximum effective temperature and the mass accretion rate appear in column 3 and 4 respectively. Since the mass accretion rate can change with time and radii, this value of M is the constant value given at the boundary. The half thickness of the disc appears in column 5. The radial extend over which the temperature of the boundary layer differs significantly from the temperature of the disc is the *thermal boundary layer*, listed ir, column 6. The radial extend over which the angular velocity in the boundary layer differs strongly from the Keplerian velocity in the disc is the dynamical *boundary layer*, which appears in column 7. In column 8 it is specified whether a thermal boundary layer is seen or not. In column 9 the inner boundary condition on the flux is specified: (I) denotes a non-flux boundary condition $dT/dr = O$, (I 1) denotes the boundary condition $F_r = \sigma T_{eff}^4$, where $T_{eff} = 5000K$.

Both viscosity prescriptions (eqs.5-6 and eqs.7-8) are used in the calculations and give the same results. Equation 9 is used in some models to prevent supersonic radial velocities to develop, this is especially useful during the relaxation of the models toward steady state. Once the steady state is reached, almost all the models exhibit highly subsonic velocities. The substitution $\nu_r = 3\nu$ is made in some cases during relaxation, for numerical convenience.

4.1 Time dependent evolution of boundary layers in YSOS

Each model is evolved from the initial condition until it r eaches a steady-sta(c. The dynamical time τ_d is of the order of a day, while the viscous time scale τ_ν varies from one model to another. As in the case of accretion disc boundary layers in Cataclysmic Variables (Godon 1995a), it is enough to follow the evolution of the models on a time scale $\tau = (\tau_d \tau_\nu)/2$. Aft,r a f,w dynamical times the models approach steady state, then they evolve slowly toward the steady stat e. As an example, in figure 2a time dependence of the luminosity $L = \int_{R_*}^{R_{out}} F_z 2\pi r dr$ is shown of model 4. It takes about onc week for the model to evolve from the initial conditions to the steady state solution. In figure 2b the maximum effective temperature is shown for model 4 as a function of time. 1 lere also the model reaches steady state after a week or so. In figu rc 2c the luminosity of model 4 is plotted against its maximum effective temperature, the circles denote the different snapshots at which the data has been collect cd. This is of course not a realistic plot in the H-R diagram, hut it gives a rough approximation of how the model relaxes from the initial condition toward the steady state. The luminosity decreases gradually while the maximum effective temperature draws characteristic z shapes. At this stage of the evolution, the accuracy of the model is of a fcw per cents, which is amply enough for the purpose of the present study. It must be stressed that the evolution of the models requires a lot of computation time, therefore, the steady st ate solutions of some models are used as initial conditions for other models. For all the models presented here, the evolution is similar to the one shown in figures 2a, 2b and 2c.

Models with very low mass acci etion rate exhibit high amplit udc oscillations of $\dot{M}$, even after they reach the steady state. In figu c 2d two snapshots of the mass accretion rate arc shown for model 4. The snapshots are taken at about one day of int erval after the model reaches steady state. The model exhibits local high amplitude variations of the mass accretion rate. As for the si mulat ion of Quasi-periodic Oscillations in Cat aclysmic Variables (CVs), Godon 1995a, these

arc oscillations trapped between the stellar surface and the reflective outer boundary, since the inflow boundary conditions are reflective. It has been shown (Yamasaki, Kato and Mineshige 1995) that such oscillations can in fact be trapped just inside the transition front between the inner hot and the outer cool regions of accretion discs in CVs and produce QPOs. In YSOs the ionization front is very small and cannot probably trap such oscillations.

The observed light curves of YSOs vary over a wide range of amplitudes and timescales (see for example Safier 1995, and the references therein). 'I'heir optical light curves have, in some cases, a periodic component which can be explained in terms of a rotating spotty stellar surface, though good temporal sampling is made difficult duc to the presence of additional irregular components. 'I'his can also be explained by the present calculations, whit]) show that low mass accretion rate discs around YSOS arc prone to exhibit high amplitude local variation of M. Again, as in the case of simulations of QPOs in CVs, the high amplitude variations of $\dot{M}$ is associated with only very small oscillation in the luminosity (few percents at most).

4.2 Steady state solutions of boundary layers in YSOs

4.2. i Variation *of* M

The effect of increasing $\dot{M}$ is first considered as all the parameters arc kept constant: $\alpha = 0.3$ and $\dot{M} = 5$ x 10-7,2.5 x 10',8.5 x 10G and 1 x $10^{-4} M_\odot/y$ (models 4,5,9 and 10). The results are shown in figures 3a-d (see also '1'able 1). For models 4,5 and 9, the results arc similar: the dynamical boundary layer extends roughly to 0.1 R_*, there is a thermal boundary layer of $\approx$ 0.3 -- $0.5R_*$ and the half thickness of the disc: $H \approx 0.1 - 0.15r$. in the low mass accretion rate regime ($M = 5 \times 10^{-7} M_\odot/y$) the temperature exceeds 70001{ on a region of roughly 0.05 R., consistent with the fitting models of observed T'Tauri spectra (Bertout et al. 1988, Hartigan et al. 1989, Basri and Bertout 1989). For the high accretion mass rate (model 10, corresponding to FUOrionis mass accretiou rate) the picture changes drastically: the dynamical boundary layer increases to 0.41?., no distinct thermal boundary layer is seen and the half thickness of the disc jumps to $0.4r$. As the mass accretion rate increases, the maximum effective temperature rises from $8000K$ ($\dot{M} = 5$ x lo-' $M_\odot/y$) up to $14000K$ ($\dot{M} = 1 \times 10^{-4}$), and as expected the spectra increase proportionally and shift to the blue (figure 3d).

'1'here arc mainly two kinds of solutions: the solutions which exhibit a thermal boundary layer component and the solutions without a thermal boundary layer.

4.2.2 Variation *of* α

In order to assess how the solutions depend on the α viscosity parameter, models are computed with different values of cr. Models 2 and 5 have the same mass accretion rate $\dot{M} = 2.5$ x $10^{-6} M_\odot/y$ but with $\alpha = 0.005$ and 0.3 respectively. Models 3 and 8 have both $\dot{M} = .5 \times 10^{-6} M_\odot/y$ but $\alpha = 0.02$ and 0.06 respectively. The results arc shown in figures 4a-d. Here also, there arc clearly two kinds of solutions: - *a) solutions with* a small dynamical boundary layer and a distinct thermal boundary layer (models 5 and 8), these solutions correspond to models with a *large* α. - h) solutions with a wide dynamical boundary layer and without thermal boundary layer (models 3 and 2), these solutions correspond to models with a relatively *small* α. The first kinds of solutions arc geometrically thiner ($H/r \approx$ O. 15) than the sec ond kind (lI/r $\approx$ 0.3). The solutions with a thermal BL have a much bluer spectrum (but a somewhat lower luminosity) than the solutions without a thermal BL (figure 4d). Here it is important to stress that for all the models with a low mass accretion rate and a flux boundary condition (denoted by 11 in column 9 of table 1), the luminosity of the computed regions exceeds the accretion luminosity. This results is consistent with the picture in which the flux boundary condition pours energy into the inner part of the disc (Regev and Bertout 1995, Godon, Regev and Shaviv 1995). This effect appears to be much stronger in YSOs than in CV systems. This effect is examined in more details in the next paragraph. It seems, therefore, that this heating process is further increased by a low value of cr. There appears to be a threshold value of α (α_{critic}) which separates the two kinds of solutions. In the present calculations, for M $\approx$ 2.5-- $5 \times 10^{-6} M_\odot/y$, $\alpha_{critic} = 0.04$. For $\alpha < \alpha_{critic}$ solutions without a thermal boundary layer arc obtained; for $\alpha > \alpha_{critic}$ a thermal boundary layer appears in the solutions. In order to see how α_{critic} depends on the mass accretion rate, onc should make a parameter study of the models. 1 lowever, the present method is time dependent and is not well suited for a parameter study (it is highly CPU time consuming).

in the extreme case of FU Orionis stars *with* $\alpha = 10^{-3}$,10 "-4 and $M = 10^{-4} M_\odot/y$, the model develops a sub-Keplerian rotation law in all the computational domain, up to the outer boundary ($r = 2R_*$). Even in the case $R_{out} = 5R_*$ the solution exhibits a non-Keplerian rotation law clOsc to the outer boundary. 1 lowever, the outer boundary conditions imposed are that of a Keplerian disc, and since the spectral methods arc very sensitive to *wrong* boundary conditions, the model can not be relaxed toward steady state. Furthermore, the numerical code presented here is highly CPU time consuming, therefor c, the outer boundary can not be moved further outward (with the same resolution).

4.2.3 The effect oj the flux boundary conditions

The effects of the inner flux boundary condition on the solutions is examined her-c for several models. Models 6 and 7 have the same values of the parameters with a high accretion mass rate, but model 6 has the boundary condition $F_* = \sigma T_{eff}^4$, while model 7 has $dT/dr = O$. Both models exhibit no thermal boundary layer and the different boundary conditions in fact c1o not affect the t-molts. At lower mass accretion rate, however, the energy poured from the star into the BL is comparable to the accretion energy. In this case one expects the solutions to be affected by the boundary condition. In figures 5 the results of models 1 and 2 arc compared: they both have a small α and the same M. Model 1 has no flux boundary condition, and has therefore an overall lower temperature (but a somewhat higher peak temperature, characteristic of a thermal boundary layer) than model 2.1 'he results are shown in figures 5a-d. The model with no flux boundary condition (1) exhibits all the characteristics

of a solution with a thermal boundary layer. The overall luminosity of model 1 is smaller than in model 2, however the spectra is relatively bluer. Comparison with figure 4d shows that model 1 has a luminosity smaller than model 5, which corresponds to the same model but with a large α, a thermal boundary layer and a flux boundary condition.

4.2.4 Optically thin *models.*

For low mass accretion rate ($\dot{M} \approx$ 10-"7 $M_\odot/y$) and non flux boundary conditions, very cool solutions are obt aincd. In these solutions, the inner part of the disc (the I\ I,) has a mid-plane (central) temperature of a few 10^4K, while the outer part of the computational domain is characterized by an extremely low mid-plane temperature of a few thousands K only. "1'here is a net transition from one region to the other (see model 11 in figures 6a and 6b). In the hot region the gas is fully ionized, while in the cool region the gas is completely neutral. The two regions arc separated by a sharp transition zone: the ionization front. The medium becomes optically thin in the outer region just adjacent to the ionization front, while it is optically thick ever.ywl)ere else. All the other n models (1 through 1 O) arc m uch warmer, completely ionized and optically thick. 1 lowever, the evolution of the cool models (1 1 and others not shown here) cannot be followed for a long time. These models are strongly unstable. It is not clear what is the exact source of the instability, but several reasons can be invoked: thermal instability from the ionization front, numerical instability due to the sharp (one grid point) transition and instability duc to high oscillation of $\dot{M}$ as in model 4 (model 11 is comp uted from model *4*, try changing the inner boundary condition). It is not clear also whether this model reached a steady state. One should therefore consider the results of model 1 1 with restrictions.

5 DISCUSSION AND CONCI.US1ON

5.1 TTauri systems.

Modeling of accretion disc boundary layers around TTauri stars ($\dot{M}$ around $10^{-6} M_\odot/y$) leads basically to two kinds of solutions. The first kind of solutions is obtained for a value of $\alpha \approx 0.1$ anti is characterized by a distinct thermal boundary layer component of extend $\Delta R_T \approx$ 0.3 — 0.5, while the dynamical boundary layer $\Delta R_D \approx$ 0.1, and n/r $\approx$ 0.1 –0.15 (consistent with the results of Popham et al. 1993, but larger than the values obtained by Lioure and Le Contel 1994, Regev and Bertout 1995). This solution is further favoured when a non-flux boundary condition is imposed at the inner boundary. The second kind of solutions is obtained assuming a small value of α ($\alpha \approx 0.01$) and is characterized by a large dynamical boundary layer $\Delta R_D \approx$ 0.5 and 11/r $\approx$ ().3, without a distinct thermal boundary layer component. In this case the maximum peek effecti ve temperature is smaller and the spectrum shows much less blue excess than the first solution. The observations seem to favoured the first kind of solutions with a rather high value of α, while modeling of FU Orionis outbursts (from a quiescent TTaur i star) infers α = 10-3, characteristic of the second kind of solutions. However, one should keep in mind that the α viscosity prescription *is an ad hoc assumption, and should* there fore be considered with restriction. In the limit of low mass accretion rate (M $\approx$ 5-- 50 x 10-7 $M_\odot/y$) peek temperatures arc obtained $7000K < T_{BL} < 11000K$ on a small radial extend, consistent with the models of TTauri spectra (Bertout et al. 1988, Hartigan et al. 1989, Basri and Bertout 1989, Hartigan et al. 1991, Bouvier and Bertout 1992 and Bertout et al. 1993) and steady state calculations (Popham et al. 1993). It further appears that there is a threshold value of α (α_{critic}) which separates the two kinds of solutions. For $\alpha > \alpha_{critic}$, solution with a distinct thermal boundary layer component arc obtained, while $\alpha < \alpha_{critic}$ leads to solutions without a thermal boundary layer. In the present calculations $\alpha_{critic} \approx$ 0.04 when M $\approx$ 2.5 — 5 x $10^{-6} M_\odot/y$. The flux boundary condition $F_r = \sigma T_{eff}^4$ leads to hotter solutions and consequently to higher values of α_{critic} than the non-flux boundary condition $dT/dr = 0$.

5.2 FU *Orionis* systems.

In the extreme case of FU orionis systems (with M = $10^{-4} M_\odot/y$), also two kinds of solutions arc obtained for the inner part of the accretion disc. These solutions again depend on the value of the α viscosity parameter. For $\alpha \approx 10^{-1}$ the inner disc is Keplerian (down to a tiny dynamical boundar y layer, close to the stellar surface) and reaches a maximum effective temperature $T \approx 13000 - 15000K$ (see also Popham et al. 1993). When $\alpha \approx 10^{-3}$ the rotation l a w is not any more Keplerian up to several stellar radii (see also Popham et al. 1993) while the temperature drops to T' $\approx$ 9000 -- 1000OK (Popham et al. 1993 obtain a flat temperature distribution).

FU Orionis outbursts modeling (Bell and Lin 1994 and Bell et al. 1995) infers α = 10-3 , 10--4, however, they assume a Keplerian rotation law down to the stellar surface. The rlon-Kepler ity of the disc, however, is not believed to seriously affect the onset of the outburst or the decay from outburst. Moreover, radial pressure profiles during outburst ($\dot{M} \approx 10^{-7} M_\odot/y$) suggest a 20-30 percent departure of the disc from Keplerity (Bell, private communication).

Standard disc modeling of spectra (Kenyon, Hartmann and Hewett 1988) derives $T_{eff}^{Max} \approx$ 7000{, based on the effective temperatur e distribution (Pringle 1981):

$$T_{eff}(r) = \left\{ \frac{3GM\dot{M}}{8\pi r^3 \sigma} \left[1 - \left(\frac{R_*}{r} \right)^{1/2} \right] \right\}^{1/4}, \qquad (16)$$

assuming a fully *Keplerian* rotation law down to the stellar surface. AI I bough the modeling of the inner part of the disc is omitted, the above fiat temperature distribution through the inner r egion of the disc is however consistent with the observed spectra of FU Orion is, therefore suggesting that a small value of α should be adopted in the numerical calcu-Miens.

5.3 Optically thin BLs in pre-main sequence stars.

Models with M $\approx$ 5 x $10^{-7} M_\odot/y$ and non-flux inner boundary condition (as well as models not presented here with $\dot{M} \approx 10^{-7} M_\odot/y$) exhibit very cool solutions. The mid plane temperature in the ionized BL reaches only a few 104 K, while the rest of disc, completely neutral, has a temperatur e of just a few $10^3 K$. The two regions are separated by

a sharp ionization front. In this case the outer region just adjacent to the ionization front becomes optically thin with an optical depth $\tau = \kappa\rho H \approx 10^{-1}$, consistent with the estimates of Bertout et al. *(1988),* Basri and Bertout (1989) and Hartigan et al (1989). These solutions exhibit high amplitude local oscillations of $\dot{M}$ during relaxation and become unstable. It is not clear whether these models reach steady state. For all the cool models computed here, the BL region is always hot enough to allow ionization of the Hydrogen, therefore leading to an ionization front always adjacent to the outer region of the thermal BL. The hotter models (models 1-10), which do not exhibit a temperature below $10^4 K$ in the computational domain, are expected to have an ionization front far from the stellar surface, at ≈ a few 10 solar radii (equivalent to ≈ 3 stellar radii, see also Bell et al. 1995), where the temperature in the disc drops below $10^4 K$. This is partly supported by the following consideration. In figure 7 some of the models are drawn in the temperature-density plane, divided in mainly two regions: the right part corresponds to a fully ionized hydrogen gas, the left part corresponds to neutral hydrogen. The two parts are separated by a thin transition region where the gas is partially ionized. Models 1-10 appear in the fully ionized region. Model 11 has its BL in the ionized part and its cooler disc in the neutral part, the sharp ionization front spreads over the entire transition region and is characterized by a jump of about one order of magnitude in both temperature and density. Models 1,4,5,8 and 9 have a distinct thermal boundary layer component and are not very warm. They are just adjacent to the partially ionized (unstable) region, the ionization front is probably located at a few stellar radii at most. Models 2,3,6,7 and 10 are relatively hotter and do not exhibit any thermal boundary layer component. They are much farther from the partially ionized region, their ionization front is certainly far from the stellar surface, at some radii $r > 10 R_*$ (the density and temperature in the disc change very slowly, therefore the outer part of the disc will appear in the plane as a tiny tail). The heating effect of the inner radial flux boundary condition on the solutions is clearly seen as a shift of the curve in the horizontal direction.

In this work, one-dimensional time dependent numerical calculations of accretion disc boundary layers around young stellar objects have been carried out, and have shown how the solutions vary according to the values of the α viscosity prescription, the mass accretion rate and the boundary conditions. The present calculations were limited to stable steady state solutions of moderate accretion rate. The difficult region of the unstable ionization front (partially ionized hydrogen region) was resolved for a few dynamic times only. It seems that, in this regime of temperatures, a more refined numerical method (with an adaptable grid) might be needed to resolve the transition region, and follow the evolution of the instability. We are presently working to improve the present numerical code (and the physical assumptions), and we hope to be able to follow the evolution of these unstable models. Results will be published elsewhere.

ACKNOWLEDGEMENTS

I thank David Meier for several discussions. I am also grateful to Robbins Bell for some comments. Robbins Bell and David Koerner kindly provided me with preprints of their papers prior to publication. Most of the numerical calculations presented in this work were performed on the JPL/Caltech CRAY Y-MP C90/232, a part of the work was however carried out on SPARCstations Sun, SS 10-30 and Sun 4-60. The Cray Supercomputer used in this investigation was kindly provided by funding from the NASA Offices of Mission to Planet Earth, Aeronautics, and Space Science. This work was performed while the author held a National Research Council (NASA Jet Propulsion Laboratory) Research Associateship. This research was carried out at the Jet Propulsion Laboratory, California Institute of Technology, under contract to the National Aeronautics and Space Administration.

REFERENCES

Basri G., & Bertout C., 1989, ApJ, 341, 340.
Bell K. R., Lin D. N. C., & Ruden S. P., 1991, ApJ, 72, 633.
Bell K. R., & Lin D. N. C., 1994, ApJ, 427, 987.
Bell K. R., Lin D. N. C., Hartmann L. W., & Kenyon S. J., 1995, ApJ, 444, 376.
Bertout C., Basri G., & Bouvier J., 1988, ApJ, 330, 350.
Bertout C., Bouvier J, Duschl W. J., & Tscharnuter W. M., 1993, A & A, 275, 236.
Bouvier J., & Bertout C., 1992, A & A, 263, 113.
Canuto C., Hussaini M. Y., Quartcroni A., & Zang T. A., 1988, Spectral Methods in Fluid Dynamics', Springer Verlag, New-York,
Clarke C. J., Lin D. N. C., & Papaloizou J. C.B., 1989, MNRAS, 236, 495.
Clarke C. J., Lin D. N. C., & Pringle J. E., 1990, MNRAS, 242, 439.
Godon P., Regev O., & Shaviv G., 1995, MNRAS, in press.
Godon P., 1995a, MNRAS, 274, 60.
Godon P., 1995b, MNRAS, in press.
Gottlieb D., & Orszag S. A., 1977, Numerical Analysis of Spectral Methods: Theory and Applications. NSF-CBMS Monograph n.26, Soc. Ind. and Appl. Math., Philadelphia PA.
Hartigan P., Hartmann L. W., Kenyon S. J., & Hewett R., 1989, ApJS, 70, 899.
Hartigan P., Kenyon S. J., Hartmann L. W., Storm S. E., Edwards S., Welty A. D., & Stauffer J., 1991, ApJ, 382, 617.
Hubeny I., 1990, ApJ, 351, 632.
Kenyon S. J., Hartmann L. W., & Hewett R., 1988, ApJ, 325, 231.
Koerner D. W., Sargent I. A., & Beckwith S. V. W., 1993, Icarus 106, 2.
Koerner D. W., & Sargent I. A., 1995, AJ, 109, 2138.
Lin D. N. C., & Papaloizou J. C. B., 1985, in Protostars and Planets II, ed. D. C. Black & M. S. Matthews (Tuscon: Univ. Arizona Press), 981.
Lioure A., & Le Contel O., 1994, A & A, 285, 185.
Papaloizou J. C. B., & Stanley G. Q. G., 1986, MNRAS, 220, 253.
Popham R., Narayan R., Hartman L. W., & Kenyon S. J.,

Safier P.N., 1995, ApJ, 44, 818.
Sargent A. I., & Beckwith S. V. W., 1991, ApJ, 382, 131.
Shakura N. I., & Sunyaev R. A., 1973, A & A, 24, 337.
Voigt R. G., Gottlieb D., & Hussaini M. Y., 1984, Spectral Methods for Partial Differential Equations, (SIAM-CBMS, Philadelphia).
Yamasaki 'J'., Kato S., & Mineshige S., 1995, PASJ, 47, 59.

FIGURES CAPTION

Figure 1.
The opacity is drawn (in cm^2/g) as a function of the temperature (Kelvin) on a log-log plot, for four different values of the density $\rho = 10^{-6}$, 10^{-7}, 10^{-8} and 10^{-9} g/cc. The temperature for which the opacity is computed is the mid-plane (central) temperature, in most of the calculations the mid-plane temperature is $T_c > 2 \times 10^4 K$ up to fews 10^5 J{.

Figure 2a.
The time dependent evolution of the luminosity of model 4. The luminosity is drawn on a log scale in erg/s.

Figure 2b.
The maximum effective temperature reaches by model 4 is drawn as a function of time. After a week or so the model approaches steady state.

Figure 2c.
The luminosity is drawn against the maximum effective temperature for model 4. The circles denote the snapshots at which the data has been collected.

Figure 2d.
Two snapshots of the local mass accretion rate are shown for model 4. The snapshots have been taken at shout onc day of interval, after the model approaches steady state (onc week). The mass accretion rate is given in solar mass per year, while the radial variable is given in units of stellar radii. nigh amplitude oscillations of the mass accretion rate appear locally during relaxation of the model toward steady state.

Figure 3a.
The angular velocity $log(\Omega(r)/\Omega_K(r))$ is plotted as a function of the radius $log(1 + 10^5(r - \{.)/\mathrm{Ii.})$, for four different mass accretion rates $\dot{M} = 5 \times 10^{-7}$, 2.5×10^{-6}, 8.5×10^{-6} and $10^{-4} M_O/y$. The alpha viscosity parameter is $\alpha = 0.3$. The width of the dynamical BL increases with increasing mass accretion rate.

Figure 3b.
The effective temperature T_{eff} is drawn as a function of the radius r/R_* for four different mass accretion rates $\dot{M} = 5 \times 10{-}7, 2.5 \times 10{-}6, 8.5 \times 10^{-6}$ and $10^{-4} M_\odot/y$. The temperature is given in Kelvin. The alpha viscosity parameter is $\alpha = 0.3$. As the mass accretion rate increases, the width of the thermal BL expends and the temperature increases. In the extreme case $\dot{M} = 10^{-4}$ the thermal BL component disappears, while the temperature raises up to more than 104 I{.

Figure 3c.
The vertical extension of the disc 11/r is drawn as a function of the radius r/R. for four different mass accretion rates $M = 5 \times 10^{-7}, 2.5 \times 10^{-6}, 8.5 \times 10^{-8}$ and $10^{-4} M_\odot/y$. The alpha viscosity parameter is $\alpha = 0.3$. The vertical thickness of the disc increases with increasing mass accretion rate, however, for $\dot{M} = 10^{-4} M_\odot$/y the thickness H is of the order of r.

Figure 3d.
Black Body spectra of the inner part of the disc arc shown for the four different mass accretion rates: $\dot{M} = 5 \times 10^{-7}$, 2.5×10^{-6}, 8.5×10^{-6} and $10^{-4} M_\odot/y$. The luminosity $\lambda F(\lambda)$ is given in erg,/s and the wavelength in cm on a log-log scale.

Figure 4a.
The angular velocity is plotted as a function of the radius (log-log, as in fig.1). Models 2 and 5 have the same mass accretion rates $\dot{M} = 2.5 \times 10^{-6} M_\odot/y$, with $\alpha = 0.005$ and 0.3 respectively. Very low values of $\alpha (\alpha \approx 10^{-2} - 10^{-3})$ leads to a wide dynamical BL ($R_{dyn} \approx$ R.), while solutions with $\alpha \approx 0.1 - 1$ leads to thin dynamical BLs ($R_{dyn} \approx 0.1$ R.). Models 3 and 8 have $\dot{M} = 5 \times 10^{-6} M_\odot/y$ and $\alpha = 0.02$ and 0.06 respectively. "J'here is a threshold value of α (in the present case $\alpha_{critic} \approx 0.04$) for which the solution 'jumps' from a thin dynamical 111, to a thick one. The two solutions arc not very sensitive to the exact value of α, as far as this value dots not reach the critical value α_{critic}.

Figure 4b.
The effective temperature is plotted in Kelvin as a function of the radius r/it. for models 2,3,5 and 8. Here also wc scc two distinct solutions. Models 2 and 3 for which $\alpha < \alpha_{critic}$, have no separate thermal BL component, and arc on the average hotter than models 5 and 8 for which $\alpha > \alpha_{critic}$. Models 5 and 8 have *however a* hot thermal BL component with maxima above the maxima of models 2 and 3.

Figure 4c.
The vertical thickness of the disc is shown for models 2,3,5 and 8. Here also there is a clear distinction between the models with $\alpha < \alpha_{critic}$ (models 2 and 3) and the models with $\alpha > \alpha_{critic}$ (models 5 and 8).

Figure 4d.
Black Body spectra of the inner part of the disc is shown for models 2 and 5. The spectra of model 3 and 8 arc similar but arc not shown for clarity. The models which exhibit a distinct *thermal* boundary layer (models 5 and 8) have a much bluer component and arc less luminous than the

models without a thermal boundary layer (2 and 3). The luminosity $\lambda F(\lambda)$ is erg/s and the wavelength is in cm on a log-log scale.

Figure 5a.
The angular velocity for models 1 and 2. Model 1 has the boundary condition $dT/dr = O$ on the stellar surface, while model 2 has $F_r = \sigma T_{eff}^4$. In model 2 the star pours energy into the BL, while in model 1 there is no influx of energy into the inner part of the disc. The dynamical BL is much more extended in model 2 than in model 1.

Figure 5b.
The effective temperature is shown for models 1 and 2. Model 1 is similar to the solutions which have $\alpha > \alpha_{critic}$ but with a more extended thermal BL. Model 2 is similar to the solutions which have $\alpha < \alpha_{critic}$. The effect of a zero flux boundary condition is to decrease the threshold value α_{critic} and to allow for the formation of a distinct thermal BL component.

Figure 5c.
The vertical thickness of the disc is shown for models 1 and 2.

Figure 5d.
Black Body spectra of models 1 and 2. The flux boundary condition imposed on model 2 leads to a much higher luminosity. Model 1 has *relatively* a stronger blue component than model 2. The luminosity $\lambda F(\lambda)$ is in erg/s and the wavelength is in cm on a log-log scale.

Figure 6a.
The mid-plane (central) temperature is shown for model 11. The temperature is given in Kelvins and the radius in stellar radii. The ionization front is located around $r \approx 1.351?$, beyond this point the temperature drops to a few thousands K (the gas is completely neutral), while in the thermal boundary layer region ($r < 1.351$,) the temperature reaches 2×10^4 (fully ionized gas). In the very inner part of the BL ($r < 1.1\ R_*$) the temperature increases further inward as one approaches the stellar surface.

Figure 6b.
The vertical thickness of the disc $H = c_s/\Omega_K$ is shown for model 11. In the thermal boundary layer the thickness reaches 0.15r while in the outer cool region it drops to 0.05r.

Figure 7.
Models 1,3, 5 and 11 are drawn in a density-temperature diagram (log-fog scale). The plane is divided in three regions. In the right part of the plane the Hydrogen is fully ionized. In the left part the Hydrogen is neutral (atoms). While in the intermediate region, Hydrogen is partially ionized. For convenience only the line which separates the fully ionized part and the partially ionized part is drawn. The line which separates the atoms from the partially ionized Hydrogen has only been drawn partially. Models 2,6,7 and 10 are similar in shape to model 3. Models 4,8 and 9 are similar to model 5. For convenience not all the models are shown. All the curves have a characteristic 'V'-shape. The upper right extremity of a V-curve corresponds to the stellar surface, the other extremity of the curve corresponds to the outer edge of the computational domain. The vertical branch of a curve corresponds to the decrease of the density in the stellar atmosphere, which reach a minimum in the boundary layer region. The horizontal branch corresponds to a decrease of the temperature as one moves from the thermal BL to the outer cooler region. The outer cooler region has a large radial extend ($r > 1.4 R_*$ in most cases) but appear on the graph as a tiny tail on the left extremity of the curve, since the density and temperature do not vary very much there. The vertical position of each model on the plane depends on the mass accretion rate, while the horizontal position depends on the temperature of the model. Model 3 represents a characteristic curve of a hot solution, without thermal boundary layer component. Model 5 represents a characteristic curve of a solution which exhibits a thermal boundary layer component. Model 1 has been obtained by imposing a non-flux boundary condition on model 2, which appears on the graph as a shift of a hot solution (3) toward the ionization line ($\log(T) = 4$, model 1). Similarly, model 11 has been obtained by imposing a non-flux boundary condition on model 4, which appears on the graph as a shift of the solution (5) to the neutral region of the plane (model 11). The curve of model 11 has been separated in four- parts (by drawing small vertical lines). The extreme left part of the curve corresponds to the outer cool region. The middle left part corresponds to the sharp transition region. The middle right part corresponds to the thermal BL region. The extreme right part corresponds to the stellar atmosphere.

TABLE CAPTION

Table 1.

Eleven different models have been computed and are listed in the table. The initial input parameters of the models are the α viscosity parameter (column 2) and the mass accretion rate (column 4). There are two different inner boundary conditions on the temperature (column 9): (I) non-flux boundary condition $dT/dr = O$, (II) $F_r = \sigma T_{eff}^4$, where $T_{eff} = 5000K$. The half thickness of the disc H appears in column 5, the radial extend of the thermal boundary layer is given in column 6 while the radial extends of the dynamical boundary layer is given in column 7. There are mainly two kinds of solutions: solutions which exhibit a distinct thermal boundary layer component and solution" which do not exhibit any component (column 8).

Table 1

(1) model	(2) α	(3) T^{eff}_{Max} $< K >$	(4) $\dot{M}$ $< M_\odot/y >$	(5) ii/r	(6) R_T/R_*	(7) R_{dyn}/R_*	(8) distinct thermal BL	(9) boundary condition
1	0.020	9100	2.5 X 10^{-6}	0.18	0.8	0.20	yes	I
2	0.005	7950	2.5 x 10^{-6}	0.25		0.50	no	II
3	0.020	8200	5.0 x 10^{-6}	0.26		0.50	no	II
4	0.300	8300	5.0 x 10^{-7}	0.10	0.3	0.10	yes	II
5	0.300	10500	2.5 x 10^{-6}	0.11	0.3	0.10	yes	II
6	0.015	8000	1.5 X10-5	0.30		0.40	no	II
7	0.015	8000	1.5 x 10^{-5}	0.30		0.40	no	I
8	0.060	10100	5.0 x 10^{-6}	0.12	0.5	0.10	yes	II
9	0.300	11700	8.5 x 10^{-6}	0.12	0.5	0.10	yes	II
10	0.300	14000	I.O X10-4	0.40		0.50	no	II
11	0.100	7300	5.0 XI O-7	0.05-0.12	0.4	0.10	yes	I

Fig 1

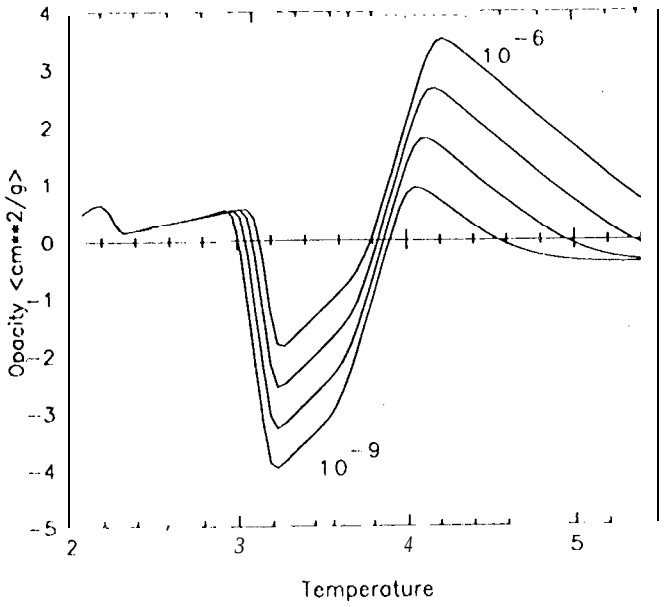

Fig 2a

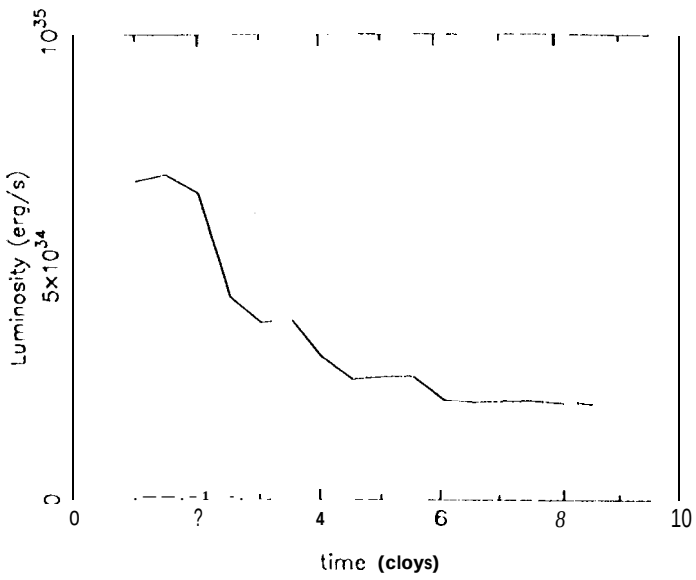

Fig 2b

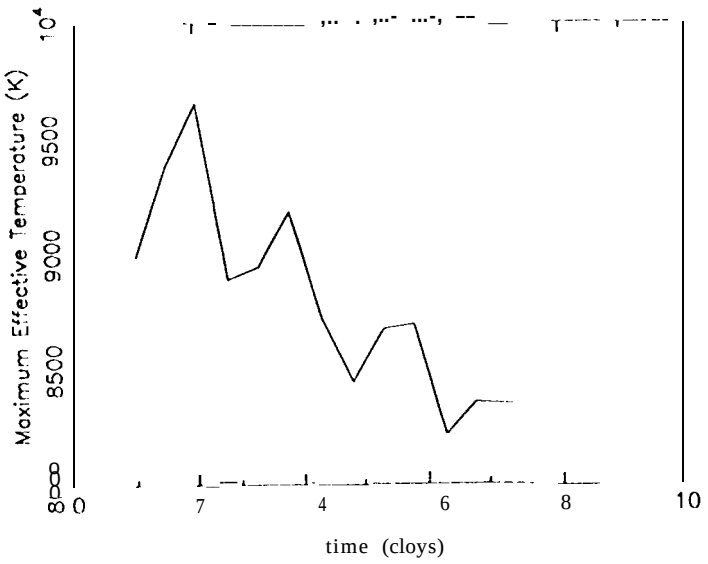

Fig 2c

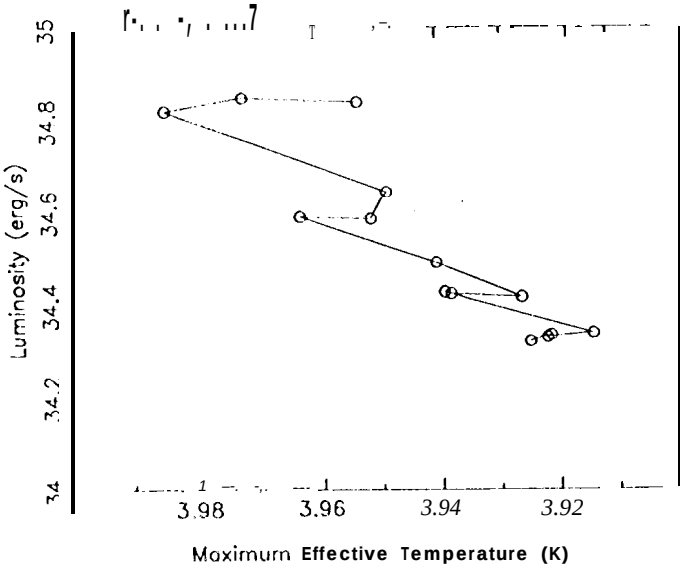

fig 2d

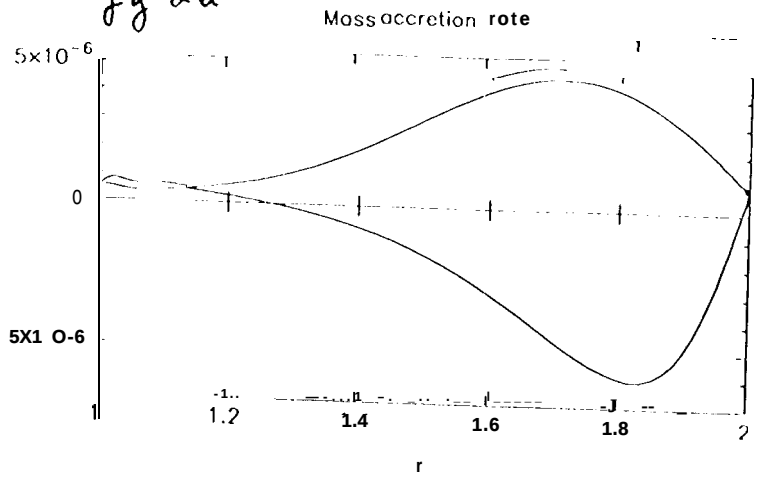

fig 3a

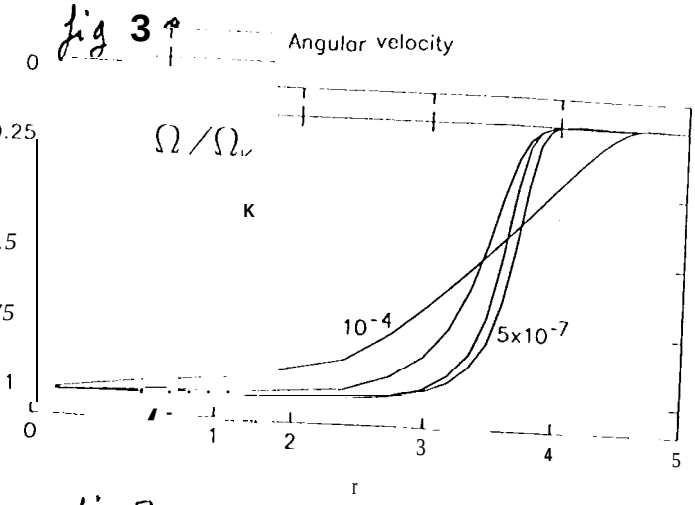

fig 3b

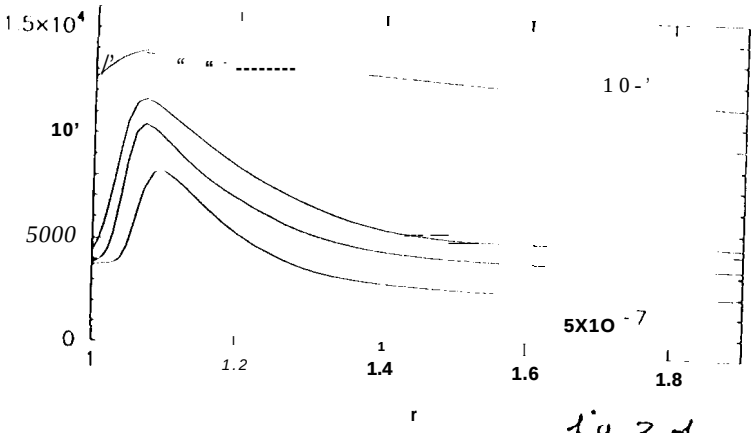

fig 3c

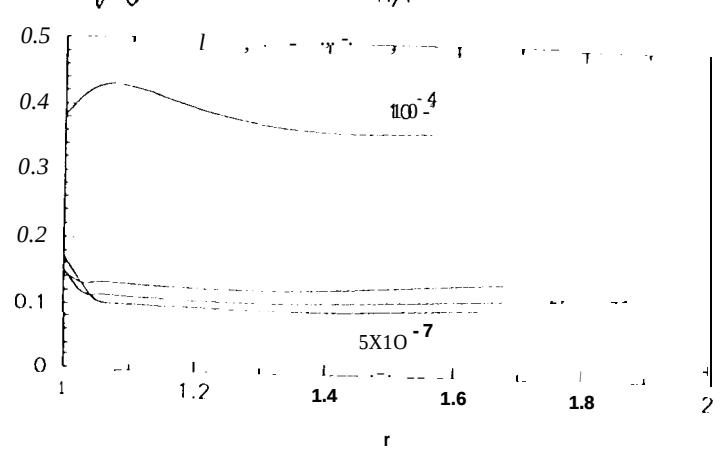

fig 3d

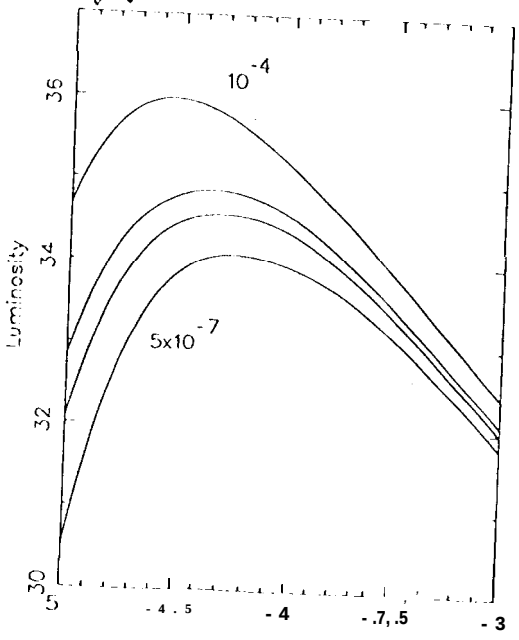

fig 4a

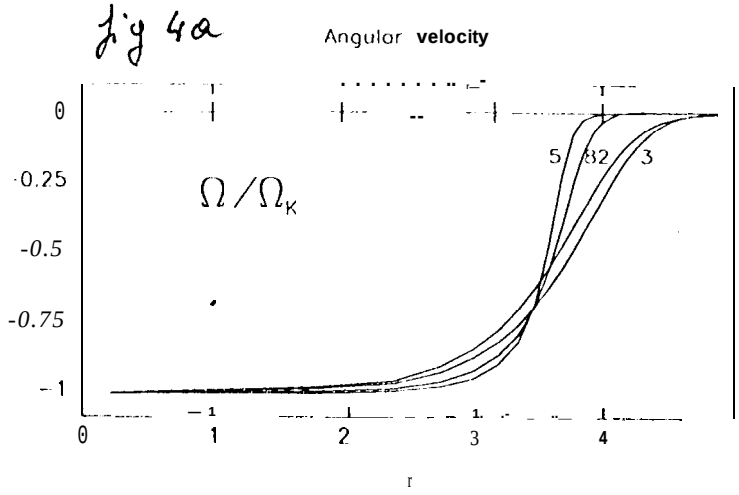

fig 4c

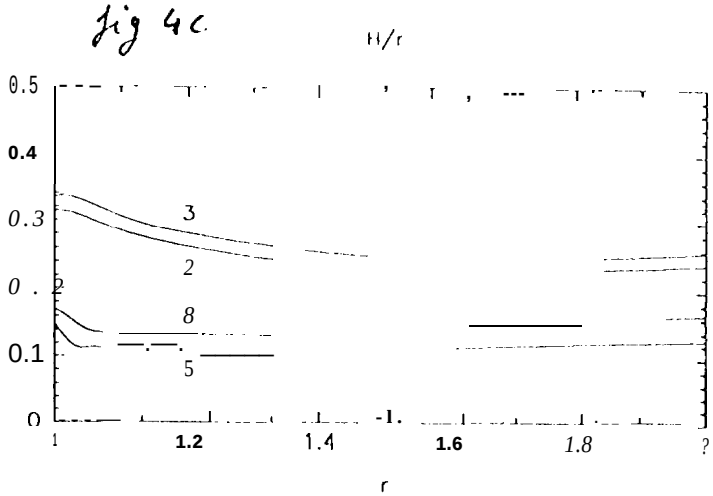

fig 4b

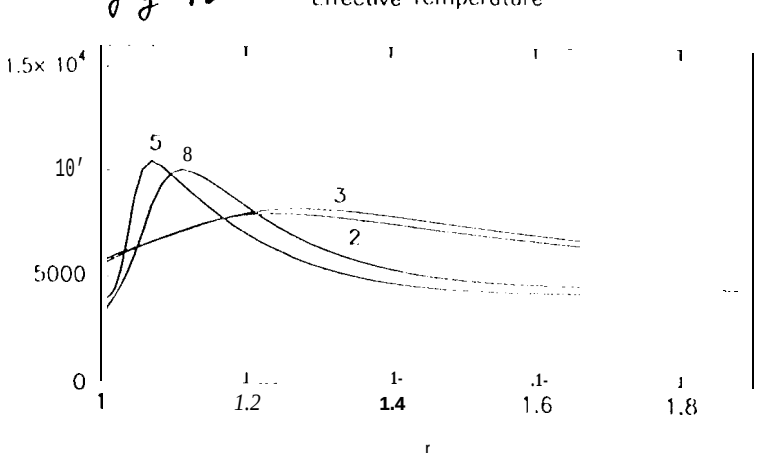

fig 4d

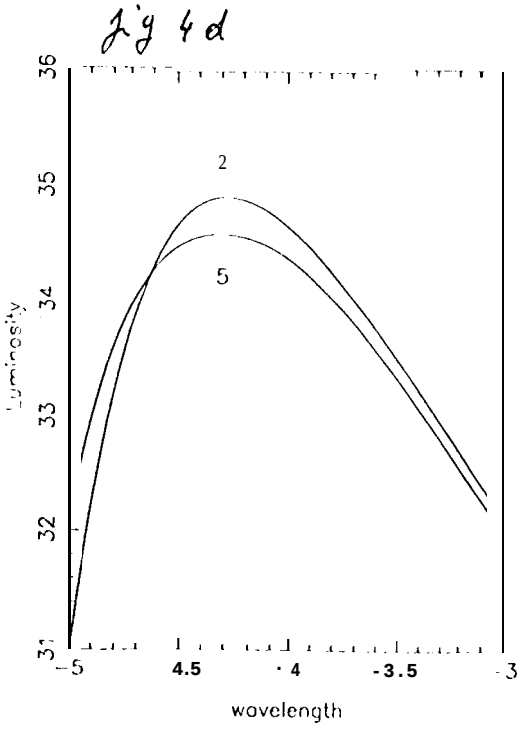

fig 5a

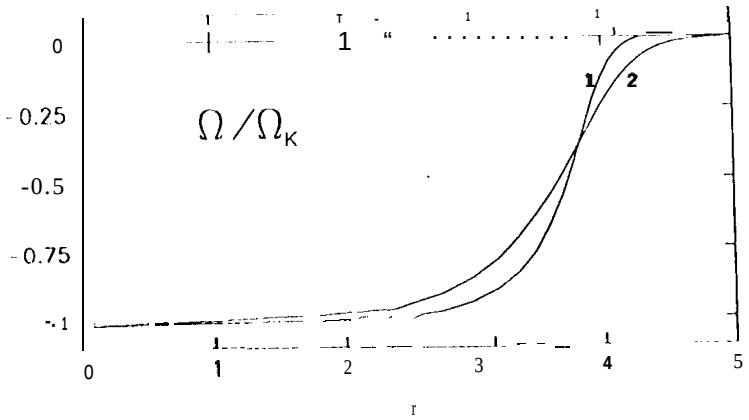

fig 5c

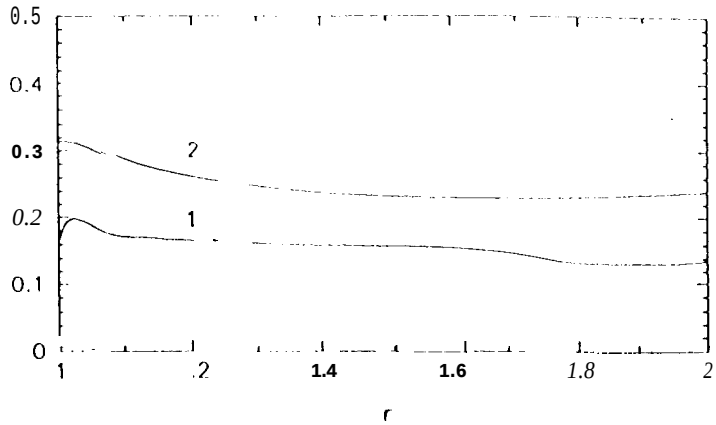

fig 5b

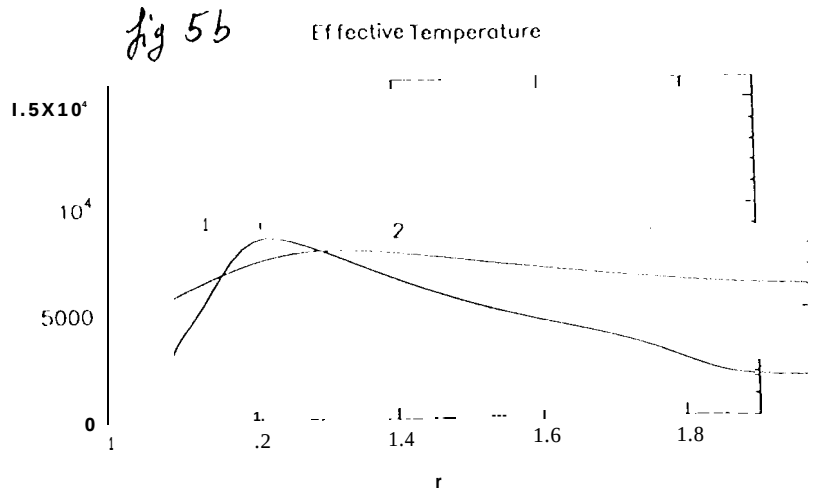

fig 5d

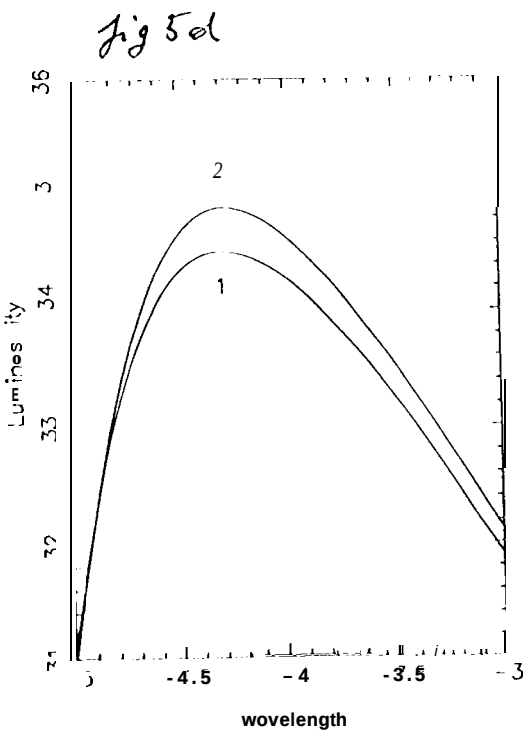

fig 6a

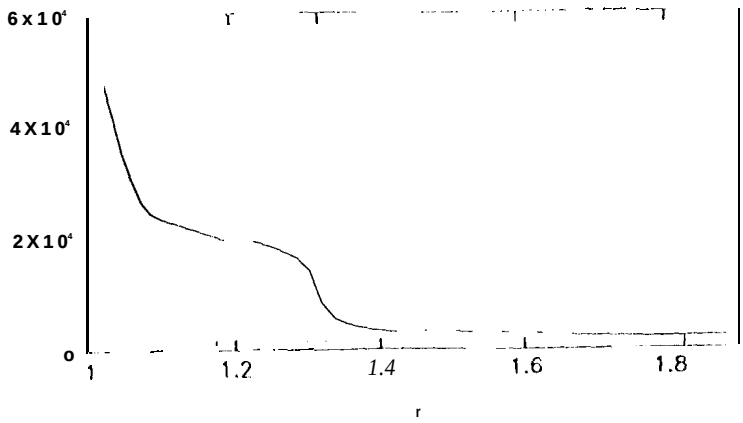

fig 6b

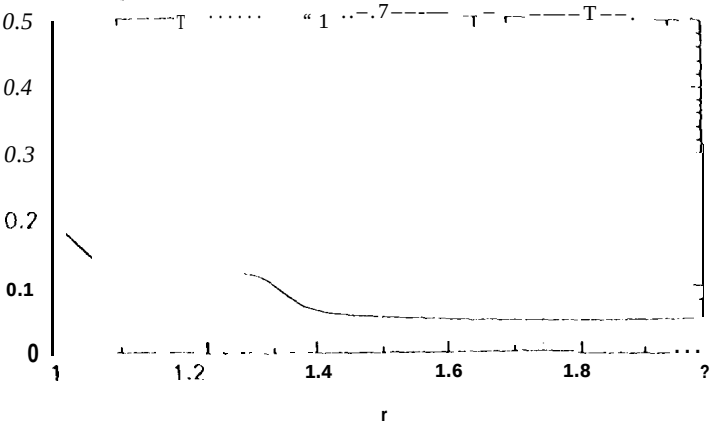

fig 7